New Calibration method to measure Rake Face Temperature of the tool during Dry Orthogonal Cutting using Thermography

D. Soler[a], P. X. Aristimuño[a], M. Saez de Buruaga[a], A. Garay[a], P. J. Arrazola[a]

[a]*Manufacturing Department, Faculty of Engineering-Mondragon Unibertsitatea, Mondragon, Spain*

Abstract

A new method for measuring temperature in the rake face of a tool during dry orthogonal cutting using thermography is presented. In addition, a new technique is also used to calibrate the infrared camera. Using this technique, real temperature values from camera response are directly obtained without the need for emissivity correction. Emissivity is thus not an uncertainty source. These techniques were applied to machining AISI 4140. Rake face temperatures are reported and correlation with cutting forces outlined. The set-up effectively showed temperature distribution on the rake face.

Keywords: Temperature Measurement, Infrared Thermography, Metal Cutting, Orthogonal Cutting

1. Introduction

Heat generation occurring during metal cutting is an important factor which affects not only the properties of machined material but also tool life [1]. The temperature reached in the tool is an indirect measurement of heat produced due to the high plastic deformation of the material, and tool-chip and tool-workpiece friction [2]. This temperature has been recognized to significantly influence tool performance [3]. It is also a key to understand tool wear and final workpiece quality [4, 5]. Moreover, recent works [6] have shown good correlation between tool temperature and tool life tests.

Experimentally measured tool temperature could also be used to validate previously developed numerical models [7].

Several experimental techniques to measure the cutting tool temperature can be found in the literature. One of the most extensively used is thermocouples [8, 9]. Although thermocouples are inexpensive, they have several disadvantages: they interfere with the heat flow, have a limited transient response, and are difficult to use in order to obtain temperature gradients. Other techniques reported are those that use thermosensitive paints [10], or metallurgical methods [11]. However, due to its advantages, in the present work an infrared method, i.e. , thermography is considered.

Infrared Radiation (IR) thermometers have received great attention in recent years as devices for temperature measurement in machining processes [12, 13, 14]. The principal advantages of

Email address: dsoler@mondragon.edu (D. Soler)

this technology are (i) it is non intrusive, i.e., the IR radiation technique does not interfere with the heat flow as thermocouples do, (ii) it enables direct determination of temperature fields and (iii) it has near real-time response. However, it has some drawbacks such as (i) the difficulty to measure temperature when lubricants are employed, (ii) the equipment cost and (iii) defining an appropriate methodology to obtain accurate measurements. In fact, due to the difficulty of using IR techniques for measuring temperature with lubricants [15], dry cutting is the only choice considered in nearly all research works.

During cutting, the chip obstructs a clear view of the tool. This fact is reported as one of the principal disadvantages of IR techniques to measure tool-chip interface [16, 17]. In order to prevent this problem three options can be found in the literature, (i) modify tools by drilling holes to allow partial vision of tool-chip interface [18], (ii) place the camera orthogonally to the chip flow, allowing to measure the temperature of a side face of the tool [19, 20] or (iii) use transparent tools [21, 22].

In the first case, a small part of the tool-chip interface can be viewed, making difficult to deduce the temperature distribution. Moreover, this can also be considered an intrusive method. In the second case, it is clear that the measured temperature field does not correspond to the rake face. These measurements could be useful for understanding the cutting process, and to find correlations between temperature and other cutting parameters [23], however, assuming that both temperatures are equal could lead to great uncertainties [24]. Finally, in the last case, good images of tool-chip interface can be obtained. However, temperature strongly depends on contact material pair, therefore, it could be very difficult to extrapolate the results obtained to commercial tools.

The method presented in the experimental set-up section provides a new procedure to directly measure rake face temperatures, overcoming the above mentioned limitations. In the literature, a patent [25] could be found in which a similar set-up is explained and it was used by the same research group in a subsequent work [26]. However, Nomura et al. did not focused their work in temperature measurement, therefore, they did not deeply analyze IR images and no details were given of how they had obtained temperature from camera response.

When infrared thermometers are used, the calibration technique and emissivity estimation is as important as the experimental set-up. Basically, the accuracy of all known infrared techniques depend on the estimation of this parameter [27] which is the major uncertainty source [14]. In the present work, a new calibration method is outlined. Using this technique, real temperature values from camera response are directly obtained without the need for emissivity correction.

The presented method was applied to machining AISI 4140. The proposed experimental set-up (section 2) was previously tested and the results obtained were reported in a previous work [7]. However, when the new calibration method was applied, new values of temperature distributions in the rake face of the tool were obtained (section 4), revealing that some published results should be revised. Some considerations of how to interpret IR images are presented in the discussion and technical remarks section (section 5). Finally, conclusions are highlighted in the last section.

2. Experimental set-up

A dry orthogonal cutting[1] operation was performed to measure tool temperatures on the rake face.

[1] In fact, it is not purely an orthogonal operation. As mentioned in section 5.2, there is a speed variation across the tool.

2.1. Cutting conditions

The methodology outlined in this paper was applied for machining AISI 4140 (290 ± 10 HB) with an uncoated plane rake face P10 carbide tool, and an edge radius of 5 µm, a SPUN 120308 P10. The workpiece was a cylindrical tube with 50 mm external diameter and 1 mm wall thickness. The samples were held in a vertical Lagun HS 1000 vertical CNC machining center, which controlled the cutting conditions: cutting velocity (v_c) and feed rate (f). Four different cutting conditions were analyzed, corresponding to v_c of 75 and 250 m/min, and f of 0.1 and 0.2 mm/rev.

Specific cutting and feed forces were measured during every test. A 3-component dynamometer (Kistler 9121) was placed under the tool holder to record the dynamic changes in the cutting forces throughout the testing. In order to ensure edge sharpness and to avoid wear effects, a new tool insert was used for each cutting condition. Every condition was repeated at least three times in order to ensure repeatability.

2.2. Thermography

The infrared camera was mounted on a moving table of the CNC. The camera was a FLIR Titanium 550 M, with 360x256 InSb detectors (pixels) and a sensitivity (Noise Equivalent Temperature Difference or NETD) of 20 mK. This camera was equipped with a macroscopic lens giving a spatial resolution of 1 pixel = 10 µm and a narrow-band filter in the IR spectral range of 3.97-4.01 µm.

The camera detectors are excited by infrared radiation for short periods of time, Integration Time (IT); that is the infrared thermography equivalent of the optical aperture time. IT must be selected depending on radiation values of the measured surface, in order to prevent a nonlinear detector response. In some cases, with the aim to cover a large range of temperatures, several ITs are used. Typically, some preliminary tests are made to adjust appropriate ITs. In the present case, it was observed that unique IT of 200 µs was enough to measure Rake face temperature.

Finally, in order to have a good overview of temperature time evolution, it is necessary to have a capture frame rate (fr) as high as possible. However, a large fr means reducing camera field of view. In this case a fr = 832.1 Hz gave a field of view of 208x162 pixels.

The main objective of this work is to describe a method to measure the rake face temperature of the tool during orthogonal dry cutting. Figure 1 shows the installation of the IR thermometer with respect to the tool rake face.

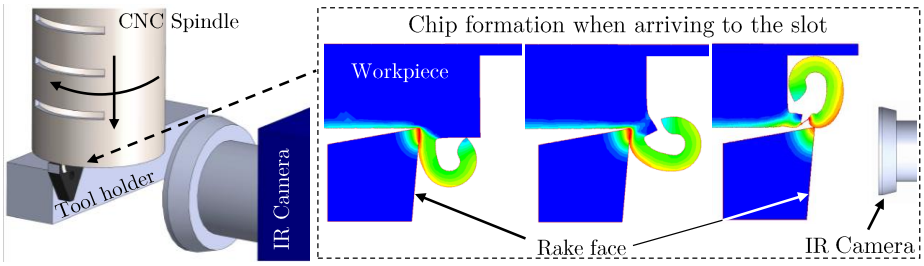

Figure 1: Installation of the IR thermometer with respect to the tool rake face; When the tool reached the slots the chip was removed and the rake face became visible.

During the cutting process, the rake face of the tool insert is hidden by the continuous chip formation. Thus, it is not possible to measure the two-dimensional temperature distribution at the

cutting edge and at the rake face. In order to prevent this problem predefined slots of θ degrees were cut across the section of the tube, see Figure 1. The cutting process was mostly divided into two steps. First, continuous machining of the tube was performed for a period of time to allow a steady state temperature to be achieved. Then, when the tool reached the slots, the tool began to cut the air instead of the workpiece, and the chip was removed. At this time the rake face and the cutting edge became visible (Figure 1). The images captured at this point were processed to obtain two-dimensional temperature distributions of the rake face during the cutting process.

Looking at a captured thermal field on the tool, see Figure 2, three zones could be distinguished: i) the chip/tool contact zone, ii) the overhang, at the right of the contact zone, and iii) the inner zone at the left of the contact zone.

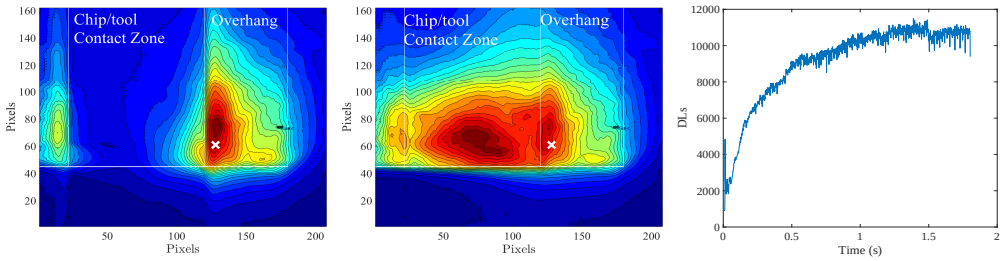

(a) (b) (c)

Figure 2: Thermography of the rake face of the tool: (a) when cutting the work; (b) when cutting the air. (c) Digital Levels (DLs) vs time of the highlighted pixel of the overhang.

Figure 2(a) shows the camera response during the cut. It is clear that it is impossible to measure the tool temperature in the contact zone due to the presence of the chip. However, it was possible to measure the temperature evolution of a fixed point in the overhang. Figure 2(c) shows Digital Levels vs Time of the highlighted pixel in Figure 2(a). Therefore, it was possible to establish if the steady state was reached. Consequently, the machining time required to reach the steady state could be determined depending on cutting conditions and materials, thus, reducing material waste.

Figure 2(b) shows the camera response when the slot was reached, i.e. when cutting the air. This thermography allowed the establishment of not only the maximum temperature in the contact zone, but also the analysis of other characteristics such as maximum position relatively to the cutting edge, temperature distribution and symmetries.

Depending on θ, fr and cutting parameters (v_c and f) different thermographies can be obtained for a single slot. With these pictures, the cooling process of the tool when cutting the air can be studied and an extrapolation can be used to estimate the temperature of the tool when it is in contact with the chip. However, in the present case, with a fr of 831 Hz, few useful pictures were obtained for each slot (in the better case 3 picture), therefore, not enough to do this extrapolation.

3. Calibration Method

Infrared cameras do not directly measure the temperature. Each camera detector, depending on the amount of photons received, returns an electrical voltage expressed by default in Digital Levels (DLs), using a transfer function known as Non Uniform Correction (NUC) [28].

The use of a blackbody makes possible [29] to relate DLs with Radiation Temperature (RT). However, a machining tool rarely could be treated as a blackbody, therefore, to obtain real Temperature (T) from RT the following equation is usually used [30].

$$\frac{1}{T} = \frac{1}{RT} + \frac{\lambda}{C_\omega} \ln(\epsilon) \tag{1}$$

where $C_\omega = 14389$ Kμm is the second radiation constant, and ϵ is the emissivity of a surface at the λ wavelength.

Therefore, the emissivity of the radiation surface is a key parameter to obtain accurate values of temperature. However, in the present case a new calibration method is presented in order to relate directly DLs with real temperature T without the need for emissivity correction (see Figure 3):

- Define a set of temperatures at regular intervals of 50 °C over a range depending on IT.
- Place the camera on a positioning table allowing its alignment and focus to desired region of the tool.
- Fill with argon the box where the tool is placed.
- Heat the tool with an induction coil in a controlled way, (tool temperature is measured with two thermocouples) and record a film at each temperature lasting for 100 frames.
- At each temperature (T), computed as the average of two thermocouples, compute the average signal in DLs.
- Use pairs (DL, T) to fit an interpolating function,wich corresponds to the calibration curve (see Figure 4).

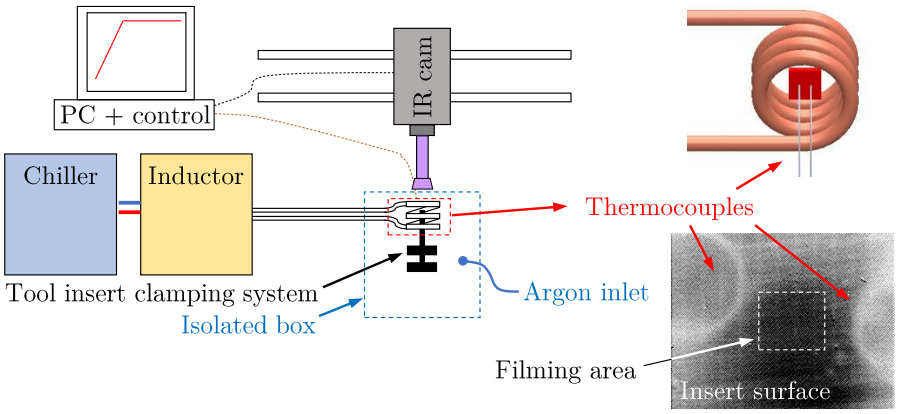

Figure 3: Experimental set-up for calibration method.

In this procedure the calibration is performed under the same experimental conditions (IT, optical path, field of view) as those used during the cutting process. Thus, the introduction of new uncertainty sources is avoided, and only those related with the cutting process itself are occurred (tool wear, oxidation and deposition).

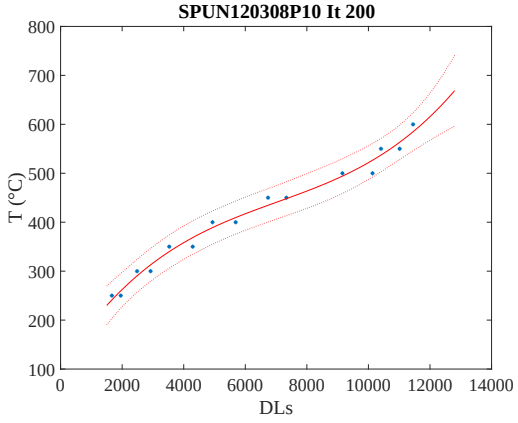

Figure 4: Relation between tool temperature an DLs when when characterizing a SPUN 120308 P10 with IT = 200 µs. Experimental data and fitted polynomial are shown.

Obviously, for every experimental test it is necessary to characterize the corresponding tool. However, the advantage of directly relating *DL*s with real temperature is that it is not necessary to estimate the emissivity.

3.1. Oxidation

As is explained in section 5 no oxidation occurred in the contact zone; however, if the heating process during the calibration is performed in presence of oxygen, the tool oxidizes.

In order to prevent this problem all characterizations were made in a controlled argon atmosphere. The LuminOx SST sensor was used to ensure that the presence of oxygen was less than 0.1%. The effectiveness of this procedure can be observed in Figure 5(a), where a new tool (left) and two tools characterized in an atmosphere with an increasing presence of oxygen (center and right) are shown. During the characterization all tools were heated over 700 °C.

The surface of these tools was evaluated in an Scanning Electron Microscope (SEM) with an Energy Dispersive X-Ray Spectrometer. The spectral composition is shown in Figure 5(b). When the presence of oxygen in the atmosphere was less than 0.1% no oxygen was observed in the tool surface.

Oxidation causes changes in surface emissivity making tool characterization unusable. See for instance Figure 6, where experimental data for two characterizations are plotted. Characterization ($c1$) was performed in a controlled atmosphere where the presence of oxygen was less than 0.1%. The other, ($c2$), was carried out with approximately 0.5% of oxygen. Both were performed with an IT of 60 µs.

For low temperatures (less than 500 °C), experimental data of both characterizations differed less than 4%. Then, due to the presence of oxygen, the tool depicted in $c2$ began to oxidize and differences grew by 85%.

4. Results

In Table 1 specific cutting and feed forces, and the maximum temperature observed in the rake face are shown. These values correspond to the mean values obtained in different repetitions

(a)

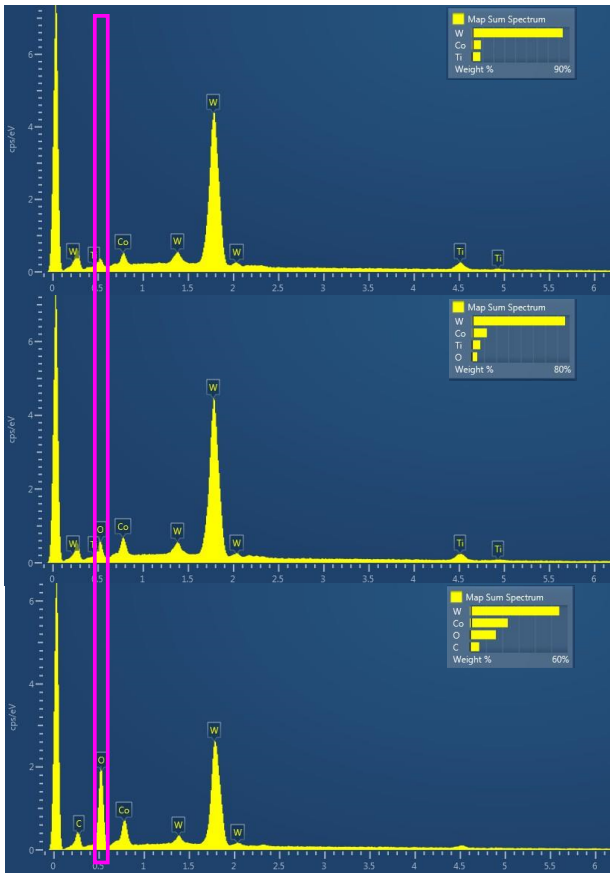

(b)

Figure 5: A controlled atmosphere of argon during the characterization reduced the oxidation of the tool, (a) shows a new tool and two characterized (heated) tools; (b) shows the spectrometry of tool surfaces after the characterization.

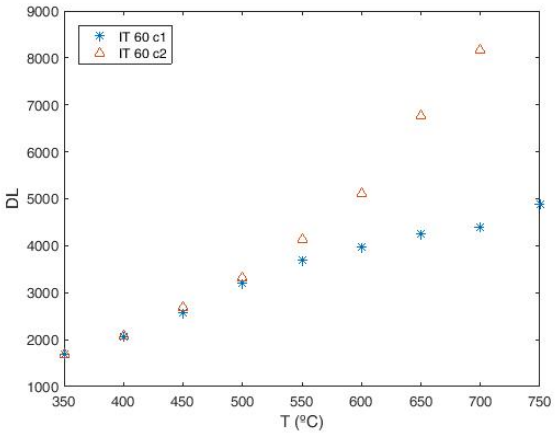

Figure 6: Experimental data for calibration of a WIDIA TPUN 160308 TTM tool with $IT = 60$ µs. Two characterization were performed with different levels of oxygen.

and the uncertainty was computed using the standard deviation σ of the experimental tests with a coverage factor of 2.

Table 1: Results of AISI 4140 experimental tests.

v_c (m/min)	f (mm)	k_c (MPa)	k_f (MPa)	T (°C)
75	0.1	2750 ± 25	1900 ± 96	370 ± 27
75	0.2	2440 ± 100	1430 ± 39	390 ± 43
250	0.1	2275 ± 100	1120 ± 54	500 ± 34
250	0.2	1990 ± 17	695 ± 18	635 ± 44

Regarding specific forces behavior, an inverse relationship between them and cutting speed was observed. In addition, as it can be noticed from the values shown in Table 1, as the feed was increased, the specific forces decreased for the same cutting velocity. In contrast, the temperature increased together with cutting velocity and the uncut chip thickness.

It is important to highlight that given values of tool temperatures do not correspond with the maximum temperature occurred during cutting. Presented temperatures are the maximum observed when there is no contact between the tool and the chip.

In order to have a clear view of the rake face, no chip could be retained between the tool and the camera. In all performed tests, it was not possible to see the rake face the first time the tool reached the slot, and therefore, some interrupted cuttings were required until a clear view was recorded. Pictures similar to shown in Figure 7(b) were obtained after several interrupted cuttings.

Figure 7(a) shows temperature vs time of two highlighted spots in Figure 7(b), one (B) placed in the overhang and the other (A) on the tool-chip contact area. Oscilations observed in Figure 7(a) were caused by the successive presence of chips between the tool and the IR camera. Red line shows an unreal temperature of the chip until rake face became visible. As shown in Figure

7(a) the temperature in the overhang during the interrupted cuts was smaller than the temperature of the steady state reached before the slot arrival. This drop was observed in different tests, and was estimated to be in the range between 50 and 100 °C.

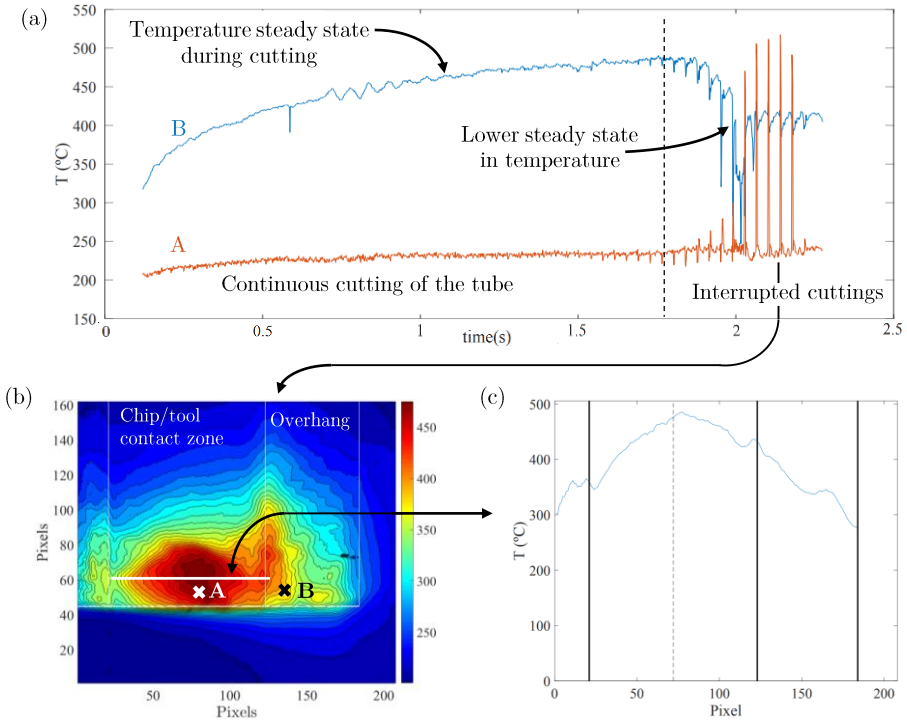

Figure 7: (a) Temperature vs. time of two highlighted pixels; (b) thermal image of the rake face cutting AISI 4140 by P-carbide, v_c = 250 m/min, f = 0.2 mm, d = 0.6 mm; (c) temperature along the path where the maximum temperature was achieved.

The temperature profile along the path, parallel to the cutting edge, where the maximum temperature was achieved is shown in Figure 7(c). The presence of two local maximums placed in the boundaries of chip/tool contact zone, as well as the slight asymmetry, was also ascertained in several tests. These phenomena are discussed in the next section.

5. Discussion and Technical Remarks

Reported temperatures were significantly smaller than those published in [7]. The main reason is that in the published work, a standard calibration of the IR camera was used to compute radiation temperature, that was subsequently corrected by applying an emissivity of 0.4. In the present case, however, using the calibration procedure outlined in section 3, tool rake face temperature T was directly obtained from camera DLs.

It is worth noting that, measured temperatures did not correspond to real cutting temperatures when tool-chip contact occurred. In addition to the effect stated in the previous section, simulations launched in AdvantEdge for different cutting conditions showed a drop in rake face temperature prior to experimental measurements.

5.1. Tool temperature drop prior to measurements

2D and 3D simulations of chip formation were launched in AdvantEdge to support a greater extension of research results concerning the tool temperature changes during exit from a cut. The cutting operation was modeled as a rigid tool interacting with a deformable workpiece, in which the tool was fixed in space, and the workpiece had a velocity equal to that of the cutting speed. The chip formation was enabled due to the remeshing algorithm integrated in the finite element code. The thermal and mechanical properties of both tool and workpiece were selected from the library of the finite element software, in which the thermal-elastic-plastic behavior of the work was modeled with the Marusich and Ortiz constitutive model [31]. The thermal diffusivity of the tool was increased from 10 to 50 mm^2/s, which was assessed to give tool maximum temperature changes with cut length qualitatively similar to results with realistic diffusivity, but with greatly reduced elapsed computing times. The Coulomb contact model was selected to govern the mechanical tool-workpiece interface behavior, while the thermal contact was assumed to be infinite. Thermal convection was set to the non-contacting surfaces of tool and workpiece to enable heat transfer with ambient.

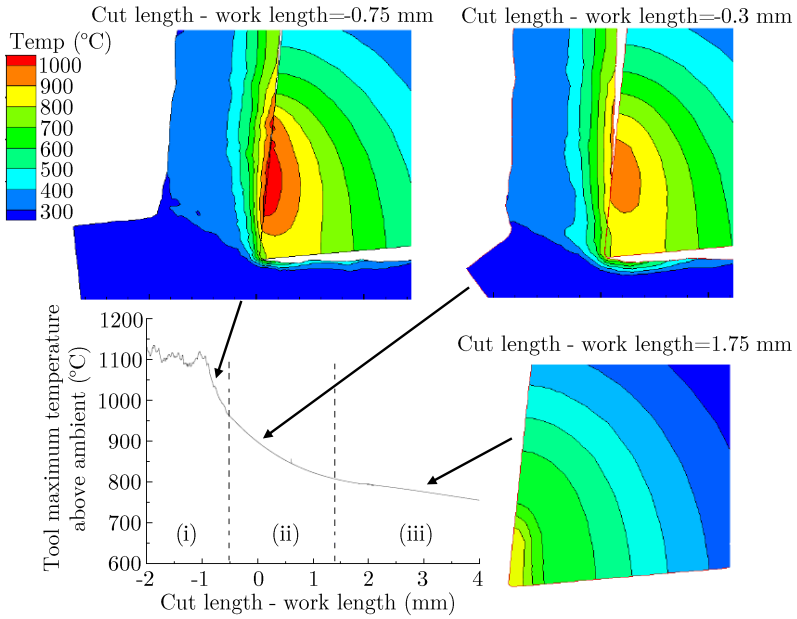

Figure 8: Examples of simulated temperature contours showing maximum temperature changes at the end of cut.

The tool temperature contours were analyzed during exiting a cut, after reaching the thermal steady state on the tool. In Figure 8, changes on the temperature contours and the evolution of tool maximum temperature depending on [cut length-work length] are plotted. It was observed that the maximum temperature on the tool rake face reduced in three main stages: i) in the first stage, the maximum temperature, which occurred away from the cutting edge, was cooled by quenching contact with the chip. The largest rate of change of temperature occurred while the maximum tool temperature was still within the chip-tool contact. The distance between the edge and the point where the maximum temperature occurred, depending on the cutting condition, was in the range of 1 to 2 times the uncut chip thickness. ii) In the second stage, the point of

maximum temperature moved away from the previous location to the edge. The rate of change of temperature in this stage reduced. iii) In the third stage, cooling continued but without position translation of maximum temperature.

These results suggested that, by the time the rake face became visible, a decrease in rake face temperature occurred. The temperature drop was found to depend on the cutting conditions, however, in most cases simulations showed that the differences between the steady state maximum temperature and the temperature at the beginning of the third stage was about 40%. Nevertheless, the exact temperature corrections suggested by simulations can not be applied directly. Other process variables such as tool-chip contact length, cutting forces and chip thickness should also be compared to the experiments in order to quantitatively validate predicted results. In any case, the authors assumed that temperature drop prior to measurement could be at least 100 °C.

Taking into account the temperature drop analyzed in the previous section concerning the lowering of steady state temperature during interrupted cutting (50-100 °C) and the drop linked to the chip exiting a cut (about 100 °C), the authors assume that temperatures during the cut would be at least 150-200 °C higher than those appearing in Table 1.

5.2. Slight Asymmetry

Two reasons can explain the asymmetry observed in Figure 7(c): i) the available area for evacuating heat is smaller on the right hand side. This is because the tool overhang on the right side was smaller than in the inside, breaking heat transmission symmetry across the tool. ii) The linear velocity of the workpiece is slightly higher on the right side due to the cylindrical form of the work.

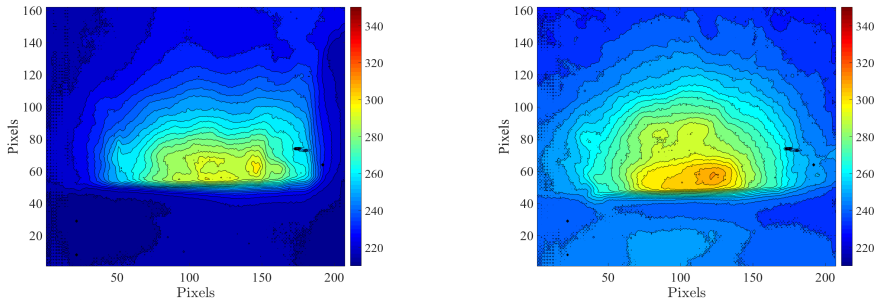

Figure 9: Rake face termographies of P-carbide when machining AISI 4140, (v_c = 75 m/min, f = 0.1 mm) (a) 0.3 mm overhang; (b) 2.3 mm.

In order to evaluate the influence of both causes, additional tests were done. The overhang was enlarged on the right side in order to place the cutting zone in the center of the tool. Results are shown in Figure 9. From this figure, it is clear that the remaining asymmetry is due to the velocity. In both cases, the temperature variations along a curve parallel to the edge was about 3% while the velocity variation was about 4%.

5.3. Local Emissivity Changes

There are some technical details that should be analyzed to avoid misinterpretations of thermographies: oxidation and material deposition.

When a metal is heated in contact with the air, it can oxidize. This oxidation yields a change in the radiating surface, and can be one of the most relevant factors conditioning an emissivity change. Focusing on the tool-chip contact area, due to the continuous sliding of the chip, it could be estimated that no oxidation occurred in this area because there was no contact with the air (Figure 2(a)). In contrast, as the inner zone and the overhang were in contact with oxygen, oxidation might occur. This was verified by observing the differences between a new and used tool, with an optical 3D measurement device (Alicona Infinite Focus IFG4), see Figure 10, in which the black area in the used tool corresponds to an oxidized surface.

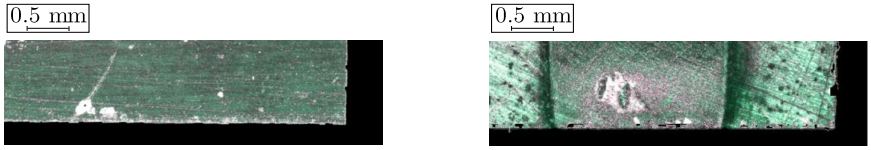

(a) (b)

Figure 10: Rake face P-carbide tool (a) shows a new tool and (b) shows a tool after cutting AISI 4140 (v_c = 250 m/min, f = 0.2 mm).

In the contact zone no black areas were observed, and therefore oxidation could be disregarded. However, in this zone work material could be deposited on the surface of the tool and modify its radiation behavior.

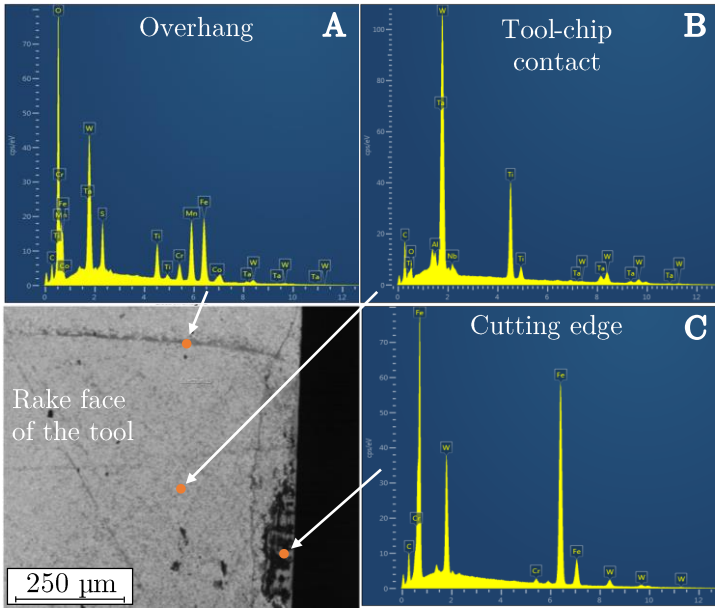

Figure 11: Rake face of used P-carbide tool obtained by a SEM and Spectral diagrams of 3 indicated points.

Figure 11 shows a used tool after cutting AISI 4140 (v_c = 250 m/min, f = 0.2 mm) and the corresponding spectral composition of three points on the rake face. In the point (A), placed in the overhang, it can be observed a significant presence of Fe and O. However, not relevant oxidation

can be observed in the chip-tool contact zone (B and C). In point B, principally, particles of W, Ti and Ta were observed, which corresponded to the substrate of the P-carbide tool employed in the tests. In some points of this zone, machined material was also observed. In point (C), placed in the near cutting edge, BUE of workpiece (mainly Fe) appeared. Oxidation and deposition alters rake face emissivity, whose effect in thermographic image analysis is discussed in next two sections.

5.3.1. Oxidation

The effect of the above mentioned oxidation could lead to a misinterpretation of thermographies. Figure 12(a), shows the temperature distribution in the rake face when machining AISI 4140 (v_c = 250 m/min, f = 0.2 mm), and the temperature profile along the path line parallel to the tool edge Figure 12(b).

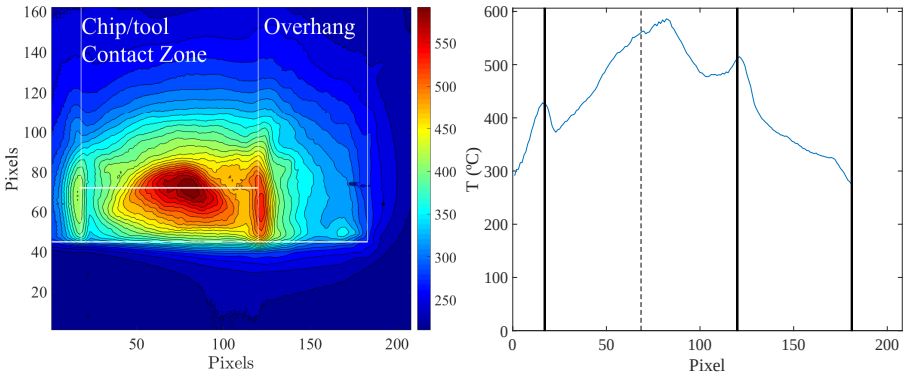

Figure 12: (a) Temperature of the rake face when machining AISI 4140 by P-carbide, (v_c = 250 m/min, f = 0.2 mm); (b) temperature profile of the straight line parallel to tool edge highlighted in (a).

Apart form the overall maximum temperature in the mid-plane of the contact zone, other two local maximums in the vicinities of the chip/tool contact zones were observed. These maximums were linked to a local emissivity increase generated by the oxidation effect which gave non realistic temperature values.

5.3.2. Deposition

The contact between chip and tool during the cutting process could lead to deposition phenomena. As can be seen in Figure 11 this possibility became fact when machining AISI 4140 at v_c = 250 m/min and f = 0.2 mm/rev.

Material deposited on the tool rake face altered the radiation condition of the measured surface. In practice, deposition causes a change in the face emissivity that if not corrected, could lead to a misinterpretation of thermographic images.

In Figure 13(a) the thermography of the above mentioned case is shown. When machining AISI 4140 by P-carbide, with v_c = 250 m/min, f = 0.2 mm. In most of the cases the maximum was placed roughly at 0.25 mm above the cutting edge (see for instance Figure 12(a)). However, in the case of the Figure 13(a), the maximum seems to be located closer to the cutting edge (11 pixel = 0.11 mm).

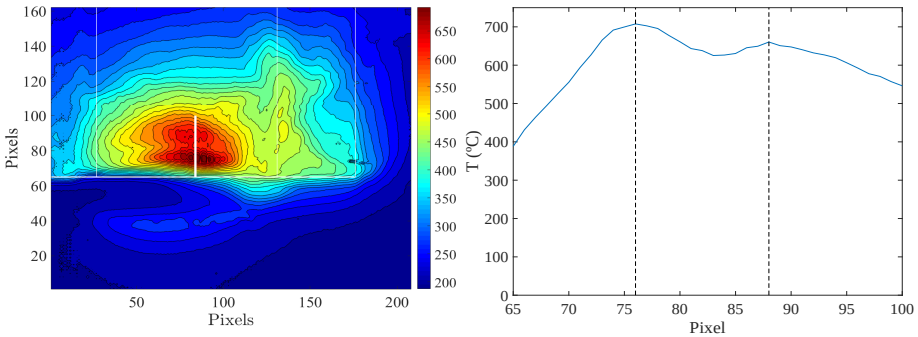

(a) (b)

Figure 13: Termography of the rake face when machining AISI 4140 by P-carbide, (v_c = 250 m/min, f = 0.2 mm). (b) temperature profile of the straight line orthogonal to the tool edge highlighted in (a).

When analyzing the temperature profile (Figure 13(b)) of the vertical path highlighted in Figure 13(a), two local maximums were observed. One placed at 0.23 mm above the cutting edge, as expected, and the other placed at 0.11 mm. This maximum was identified as not real. The presence of steel deposition in this area implied a local increase of the emissivity that yielded to an overestimation of temperature.

6. Conclusions and Further Work

An experimental set-up to measure the tool temperature during dry orthogonal cutting using infrared techniques has been described. The present work analyzed the case when machining AISI 4140. However, the same procedure can be followed for other materials.

Applying this new method tool rake face temperature can be measured. In addition, tests can be performed with smaller material waste as the steady state in the rake face is reached faster than in the side face.

Furthermore, the presented procedure enables the analysis of the shape of the temperature distribution as well as to determine the maximum temperature.

Measurements carried out reveal that the peak temperature increased with the cutting velocity and the feed. However, specific forces had an inverse relationship to cutting speed and feed.

The effect of local emissivity changes due to oxidation and material deposition in the rake face are also discussed.

Using the calibration process described in section 3, temperature can be directly obtained from camera response without the need of emissivity correction, thus, eliminating emissivity as a source of uncertainty. This calibration process can be implemented with new or used tools, and can prevent mistakes in temperature estimation due to material deposition, wear and/or tool oxidation. However, the set-up must be improved in order to ensure a more uniform heating of the tool when calibrating, otherwise, it is not possible to systematically correct above mentioned mistakes.

Future work will attempt to optimize i) workpiece, by increasing diameter, to ensure the steady state to be reached even during the interrupted cutting and ii) the slots geometries and camera resolution, by increasing the frame rate, in order to get more pictures of the rake face

when cutting the air. This would enable to perform an extrapolation to estimate the temperature of the tool when it is in contact with the chip. Moreover, it would be interesting to synchronize force signals and thermal video in order to estimate the exact time-lapse between the exit from a cut and the first useful thermal image.

In addition, if the calibration method presented in this research is applied to focus on a blackbody, it would be possible to estimate the emissivity of the tool. Further work will attempt to implement this idea to estimate the emissivity of different materials. While in the context of the present work this is not a relevant parameter, the authors consider it could be interesting for the research community.

Tool oxidation was observed when heating the tool in presence of oxygen, however this phenomena could be prevented by controlling the atmosphere. It is the opinion of the authors that using the described calibration method it could be possible to learn more about oxidation, and its relationship with temperature and time.

Acknowledgements

We would like to express our very great appreciation to Dr. Tom Childs for his valuable and constructive suggestions during the planning, development and discussion of this research work, and for his support with the AdvantEdge simulations.

This work was supported by the Basque Government within the project MICROMAQUINTE (PI_2014_1_116) and the Spanish Government within the project EMULATE (DP12015-67667-C3-3R).

References

[1] R. M'Saoubi, C. Le Calvez, B. Changeux, J. L. Lebrun, Thermal and microstructural analysis of orthogonal cutting of a low alloyed carbon steel using an infrared-charge-coupled device camera technique, Proceedings of the Institution of Mechanical Engineers, Part B: Journal of Engineering Manufacture 216 (2002) 153–165.

[2] G. L. Coz, M. Marinescu, A. Devillez, D. Dudzinski, L. Velnom, Measuring temperature of rotating cutting tools: Application to {MQL} drilling and dry milling of aerospace alloys, Applied Thermal Engineering 36 (2012) 434 – 441.

[3] G. Sutter, L. Faure, A. Molinari, N. Ranc, V. Pina, An experimental technique for the measurement of temperature fields for the orthogonal cutting in high speed machining, International Journal of Machine Tools and Manufacture 43 (2003) 671 – 678.

[4] M. Davies, T. Ueda, R. M'saoubi, B. Mullany, A. Cooke, On the measurement of temperature in material removal processes, CIRP Annals-Manufacturing Technology 56 (2007) 581–604.

[5] I. Jawahir, E. Brinksmeier, R. M'Saoubi, D. Aspinwall, J. Outeiro, D. Meyer, D. Umbrello, A. Jayal, Surface integrity in material removal processes: Recent advances, CIRP Annals-Manufacturing Technology 60 (2011) 603–626.

[6] D. Soler, P. Aristimuño, A. Garay, P. Arrazola, F. Klocke, D. Veselovac, M. Seimann, Finding correlations between tool life and fundamental dry cutting tests in finishing turning of steel, Procedia Engineering 132 (2015) 615 – 623.

[7] P. J. Arrazola, P. Aristimuno, D. Soler, T. Childs, Metal cutting experiments and modelling for improved determination of chip/tool contact temperature by infrared thermography, {CIRP} Annals - Manufacturing Technology 64 (2015) 57 – 60.

[8] H. Ay, W.-J. Yang, Heat transfer and life of metal cutting tools in turning, International Journal of Heat and Mass Transfer 41 (1998) 613–623.

[9] D. Stephenson, Tool-work thermocouple temperature measurements theory and implementation issues, Journal of Manufacturing Science and Engineering 115 (1993) 432–437.

[10] S. Rossetto, U. Koch, An investigation of temperature distribution on tool flank surface, Annals of the CIRP (1970) 551–557.

[11] E. M. Trent, P. K. Wright, Metal cutting, Butterworth-Heinemann, 2000.

[12] R. Dewes, E. Ng, K. Chua, P. Newton, D. Aspinwall, Temperature measurement when high speed machining hardened mould/die steel, Journal of Materials Processing Technology 92-93 (1999) 293 – 301.
[13] P. Arrazola, I. Arriola, M. Davies, A. Cooke, B. Dutterer, The effect of machinability on thermal fields in orthogonal cutting of AISI 4140 steel, CIRP Annals-Manufacturing Technology 57 (2008) 65–68.
[14] M. Davies, H. Yoon, T. Schmitz, T. Burns, M. Kennedy, Calibrated thermal microscopy of the tool–chip interface in machining, Machining science and technology 7 (2003) 167–190.
[15] M. Cuesta, P. Aristimuño, A. Garay, P. Arrazola, Heat transferred to the workpiece based on temperature measurements by ir technique in dry and lubricated drilling of inconel 718, Applied Thermal Engineering 104 (2016) 309–318.
[16] C. Dinc, I. Lazoglu, A. Serpenguzel, Analysis of thermal fields in orthogonal machining with infrared imaging, Journal of Materials Processing Technology 198 (2008) 147 – 154.
[17] B. Müller, U. Renz, Time resolved temperature measurements in manufacturing, Measurement 34 (2003) 363–370.
[18] M. Al Huda, K. Yamada, A. Hosokawa, T. Ueda, Investigation of temperature at tool-chip interface in turning using two-color pyrometer, Journal of manufacturing science and engineering 124 (2002) 200–207.
[19] J. Artozoul, C. Lescalier, O. Bomont, D. Dudzinski, Extended infrared thermography applied to orthogonal cutting: Mechanical and thermal aspects, Applied Thermal Engineering 64 (2014) 441–452.
[20] R. M'Saoubi, H. Chandrasekaran, Investigation of the effects of tool micro-geometry and coating on tool temperature during orthogonal turning of quenched and tempered steel, International Journal of Machine Tools and Manufacture 44 (2004) 213 – 224.
[21] J. Heigel, E. Whitenton, B. Lane, M. Donmez, V. Madhavan, W. Moscoso-Kingsley, Infrared measurement of the temperature at the tool-chip interface while machining ti-6al-4v, Journal of Materials Processing Technology 243 (2017) 123–130.
[22] J. C. Garcia-Gonzalez, W. Moscoso-Kingsley, V. Madhavan, Tool rake face temperature distribution when machining ti6al4v and inconel 718, Procedia Manufacturing 5 (2016) 1369–1381.
[23] M. Armendia, A. Garay, A. Villar, M. Davies, P. Arrazola, High bandwidth temperature measurement in interrupted cutting of difficult to machine materials, CIRP Annals-Manufacturing Technology 59 (2010) 97 – 100.
[24] D. Soler, T. H. C. Childs, P. J. Arrazola, A Note on Interpreting Tool Temperature Measurements from Thermography, Machining Science and Technology 19 (2015) 174–181.
[25] D. Murakami, H. Moriguchi, A. Ikegaya, Noncontact temperature distribution measuring apparatus, 2000. US Patent 6,089,750.
[26] T. Nomura, H. Moriguchi, K. Tsuda, K. Isobe, A. Ikegaya, K. Moriyama, Material design method for the functionally graded cemented carbide tool, International Journal of Refractory Metals and Hard Materials 17 (1999) 397–404.
[27] P. Herve, J. Cedelle, I. Negreanu, Infrared technique for simultaneous determination of temperature and emissivity, Infrared Physics & Technology 55 (2012) 1–10.
[28] L. Bünger, K. Anhalt, R. Taubert, U. Krüger, F. Schmidt, Traceability of a ccd-camera system for high-temperature measurements, International Journal of Thermophysics (2015) 1–19.
[29] D. Soler, P. Aristimuño, A. Garay, P. J. Arrazola, Uncertainty of temperature measurements in dry orthogonal cutting of titanium alloys, Infrared Physics & Technology 71 (2015) 208 – 216.
[30] P. Saunders, Radiation Thermometry: Fundamentals and Applications in the Petrochemical Industry, volume TT78, SPIE Press, 2007.
[31] T. Marusich, M. Ortiz, Modelling and simulation of high-speed machining, International Journal for Numerical Methods in Engineering 38 (1995) 3675–3694.